MATERIALS CHEMISTRY FRONTIERS

On Structure and Phase Transformation of Uranium Doped La2Hf2O7 Nanoparticles as an Efficient Nuclear Waste Host

Journal:	*Materials Chemistry Frontiers*
Manuscript ID	QM-RES-05-2018-000266.R1
Article Type:	Research Article
Date Submitted by the Author:	20-Jun-2018
Complete List of Authors:	Mao, Yuanbing; University of Texas - Pan American, Department of Chemistry Abdou, Maya; The University of Texas Rio Grande Valley Gupta, Santosh; BARC, Zuniga, Jose; The University of Texas Rio Grande Valley

On Structure and Phase Transformation of Uranium Doped $La_2Hf_2O_7$ Nanoparticles as an Efficient Nuclear Waste Host

Maya Abdou[1], Santosh K. Gupta[1,2], Jose P. Zuniga[1], and Yuanbing Mao[1,3]*

[1]Department of Chemistry, University of Texas Rio Grande Valley, 1201 West University Drive, Edinburg, Texas 78539, USA

[2]Radiochemistry Division, Bhabha Atomic Research Centre, Trombay, Mumbai-400085

[3]School of Earth, Environmental, and Marine Sciences, University of Texas Rio Grande Valley, 1201 West University Drive, Edinburg, Texas 78539, USA

*To whom correspondence should be addressed. E-mail: yuanbing.mao@utrgv.edu, Tel.: +1-956-665-2986.

Abstract

The design and development of efficient and stable nuclear waste hosts has drawn intensive interest for long-lived lanthanides and actinides. A detailed investigation of their structure and potential structural evolution are crucial. In this study, we have synthesized lanthanum hafnate $La_2Hf_2O_7$ nanoparticles (NPs) doped with uranium at different concentrations (0 – 10%) and investigated their structural transition. We have discovered that in our $La_2Hf_2O_7$:U NPs, the uranium dopants are stabilized at both U^{4+} and U^{6+} oxidation states in which the U^{+6} oxidation state exists in octahedral uranate UO_6^{6-} form. We also confirmed that the U^{+4} ions substituted the Hf^{4+} ions with a lifetime of ~1.0 μs and the UO_6^{6-} ions resided at the La^{3+} sites with a lifetime of ~9.0 μs. More interestingly, the proportion of the U^{4+} ions in the $La_2Hf_2O_7$:U NPs was higher than that of the UO_6^{6-} ions at low doping level, but at the doping level higher than 2.5%, the fraction of the UO_6^{6-} ions was greater than that of the U^{4+} ions. Furthermore, we studied the structural phase transformation from order pyrochlore to cotunnite of these $La_2Hf_2O_7$:U NPs with increasing uranium doping level, and found that ordered pyrochlore phase favors the U^{4+} ions whereas disordered cotunnite phase favors the UO_6^{6-} ions. We further used in-situ Raman spectroscopy to confirm the reversible cotunnite to pyrochlore phase transformation of the $La_2Hf_2O_7$:10%U NPs at 900°C. Therefore, this work demonstrated the successful development of uranium doped $La_2Hf_2O_7$ NPs and thorough characterization of the fundamental spectra of uranium ions, doping induced phase transformation, and structure-optical property correlation.

Keywords: Uranium; $La_2Hf_2O_7$; Phase transformation; Speciation; Photoluminescence

1. Introduction

Compounds with a genral formula of $A_2B_2O_7$ have received intense attention due to their high thermodynamic stability, high radiation stability, capability to incorporate lanthanides and actinides, and ability to form antisite defects by swapping A and B positions.[1-5,6] Among these compounds, rare-earth hafnates $RE_2Hf_2O_7$ possess various desirable properties, which are very important for different technological applications, such as computer tomography (CT),[7] positron emission tomography (PET),[8] high-energy radiation detectors,[9] scintillation host materials,[10] magnetic materials,[11] among others.[4, 9, 12, 13, 14, 15]

Uranium and its radioactive isotopes contribute to a high-level of nuclear waste, which needs to be properly disposed. Uranium ion has multiple oxidation states (i.e. +3, +4, +5 and +6), all of which are luminescence active with characteristics emission.[16-19] Speciation studies of uranium ion in $A_2B_2O_7$ compounds will be highly beneficial for fundamental uranium chemistry and nuclear industry. However, because of its complex nature and various existing valence states, the incorporation mechanism, oxidation state and structural environment of uranium ions in $A_2B_2O_7$ compounds are uncharted and vague. For example, Zhang and coworkers investigated the phase evolution of U doped $Y_2Ti_2O_7$ and $Gd_2Ti_2O_7$.[20] They have carried out detailed phase evolution investigation from $Ln_2Ti_2O_7$ pyrochlores to $Ln_{0.5}U_{0.5}Ti_2O_6$ (Ln = Y and Gd) brannerites in glasses using various techniques such as X-ray diffraction, Raman spectroscopy, diffuse reflectance spectroscopy and electron microscopy. Shu et al. studied the effect of alpha irradiation on U doped $Gd_2Zr_2O_7$.[21] Their study revealed that main crystal structure does not change but weak structural ordering takes place on alpha irradiation. They have also found increase in radiation stability of $Gd_2Zr_2O_7$ at high uranium concentrations. Lu *et al.* explored the effects of U_3O_8 on the phase and microstructure evolution of $Gd_2Zr_2O_7$ and found that uranium is homogenously distributed in +4 and +6 oxidation states at Gd^{3+} and Zr^{4+} sites, respectively.[22] One of us studied the speciation of uranium using luminescence spectroscopy for $A_2Zr_2O_7$ (A = La, Nd and Gd) and the results show that uranium is stabilized as U^{4+} and UO_6^{6-} in $Gd_2Zr_2O_7$, only as UO_6^{6-} in $Nd_2Zr_2O_7$, and as both UO_6^{6-} and UO_2^{2+} in $La_2Zr_2O_7$.[23-25] There are few more reports on uranium doped $Gd_2Zr_2O_7$ wherein speciation of uranium was carried out in bulk phase using X-ray diffraction, Raman spectroscopy and X-ray photoelectron spectroscopy along with other suitable techniques.[26-28] However, none of these reports includes studies on structure and phase evolution of uranium doped $La_2Hf_2O_7$ nanoparticles (NPs).

Photoluminescence (PL) spectroscopy is an indispensable technique to probe optical properties and local structure of phosphors. It is also the most acceptable technique for detecting and estimating uranium in ultra-trace level in both solids as well as aqueous media.[29] Meanwhile, Raman spectroscopy has been widely utilized as a tool to distinguish between the disordered fluorite and the ordered pyrochlore phases of $A_2B_2O_7$ compounds. Due to its high sensitivity to oxygen-cation vibrations, Raman spectroscopy has the capability to probe local structure and to further identify disorder within the pyrochlore structure, which emerge from vacancies and defects that disrupt the translational symmetry. Moreover, X-ray photoelectron spectroscopy (XPS) is a surface-sensitive quantitative spectroscopic technique that measures the elemental composition, empirical formula, chemical state and electronic state of the elements that exist within a material. It is also one of the highly sensitive methods to probe oxygen vacancies. Therefore, in this work, we have used these three techniques together along with other traditional materials characterization techniques complementarily to investigate the structure and phase transition of the $La_2Hf_2O_7$ NPs with different uranium doping levels. Lastly, for the first time, we observed reversible phase transformation in the $La_2Hf_2O_7$:10%U NPs using in-situ Raman measurement. Therefore, through the successful development of uranium doped $La_2Hf_2O_7$ NPs and their thorough characterization of the fundamental spectra of uranium ions, doping induced phase transformation, and structure-optical property correlation, we believe this work open new research areas important for safe nuclear energy and sustainable environment.

2. Experimental

Figure S1 depicts the schematic of the combined co-precipitation and molten-salt synthesis (MSS) procedure adopted to synthesize the $La_2Hf_2O_7$:xmol%U NPs (x = 0.5 - 10.0).[4, 9, 30-31] Additional synthesis and characterization details are provided in ESI (S.2.1 and S.2.2).

3. Results and discussion

3.1 Phase, Structure and morphological analysis:

XRD is used to confirm the phase of the $La_2Hf_2O_7$:x%U (x = 0, 0.5, 1, 2.5, 5, 7.5, and 10) NPs (Figure S2). Fourier transformed infrared (FTIR) spectra were collected to identify the phase and rule out the formation of any additional phase of the $La_2Hf_2O_7$:x%U NPs. Morphostructural characterization of the synthesized NPs was performed with scanning electron microscopy

(SEM) and high-resolution transmission electron microscopy (HRTEM) as shown in in Figures S4 and S5. The presence of uranium dopant was confirmed by energy dispersive spectroscopy (EDS) (Figure S6). The doping efficiency and uniform distribution of constituent element were investigated using elemental mapping (Figure S7).

3.2 Raman spectroscopy

It is well known that the ideal pyrochlore phase has six well-resolved Raman active vibrational modes in the range of 200-1000 cm^{-1} which are represented as $\Gamma_P = A_{1g} + E_g + 4F_{2g}$, whereas the fluorite phase has mainly one Raman active mode that is $\Gamma_F = F_{2g}$.[32] This is because seven oxygen ions are randomly distributed at eight anion positions, which leads to structural disordering in the fluorite phase, and hence all the fine peaks of pyrochlore collapsed into one broader peak. More specifically, phase transformation from $A_2B_2O_6O'$ pyrochlore (Fd-3m space group) to AO_2 fluorite (Fm3m, Z = 4) structure takes place through the disappearance of A_{1g} and E_g Raman modes and decrease in the number of F_{2g} modes from 4 to 1.

Radius ratio (r_A/r_B) plays an important role in determining which structure of $A_2B_2O_7$ compounds attain.[33] It has been reported that fluorite phase is more likely to form if $r_A/r_B < 1.46$ and while ordered pyrochlore phase is more likely to be stabilized if r_A/r_B is greater than 1.46 at room temperature. It was propose that r_A/r_B for different $A_2B_2O_7$ compositions follows this trend: disordered fluorite phase (DFP) $r_A/r_B < 1.21 < \delta$-phase $r_A/r_B < 1.42 - 1.44 <$ ordered pyrochlore phase (OPP) $r_A/r_B < 1.78 - 1.83 <$ monoclinic pyrochlore $r_A/r_B < 1.92$.[34] $La_2Hf_2O_7$ is the most favorable candidate with radius ratio of 1.45 to be stabilized in pyrochlore phase. **Figure 1a** shows the Raman spectra of the as-synthesized $La_2Hf_2O_7$:U NPs with different uranium concentrations. Undoped sample has six well-resolved Raman peaks at 306, 324, 402, 501, 521 and 601 cm^{-1} pertaining to the vibrations of La-O and Hf-O bonds. These peaks are assigned to F_{2g}, E_g, F_{2g}, A_{1g} F_{2g} and F_{2g} modes, respectively.[35] The vibrational modes of F_{2g}, E_g, and F_{2g} at low frequency region of 300-400 cm^{-1} arise from vibrations of the La–O and Hf–O bonds. On the other hand, the high frequency band at 501, 522 and 601 cm^{-1} arise from the stretching of the Hf–O bonds.[35] However, the complete pyrochlore phase is preserved only up to 1.0% uranium doping level. After that, the fine OPP structure starts to collapse into broader peaks and disordered fluorite phase or cotunnite phase evolves and coexists with OPP. At 2.5% uranium doping level and above, there is complete disordering of the $La_2Hf_2O_7$ pyrochlore phase and a

broad peak around 715 cm^{-1} appears. Its intensity keeps increasing and even overpowers the broad fluorite peak at 7.5% and 10% uranium doping levels. This peak is not a fundamental Raman vibrational mode of pyrochlore-structured $A_2B_2O_7$ type oxides. It is believed to appear due to the distortions of the BO_6 octahedra.[35-36] In $La_2Hf_2O_7$, it has been attributed to distortion in HfO_6 octahedra and other kind of structural defects due to doping of uranium at La/Hf site. The average metal-oxygen bond lengths in the fluorite phase is close to those existing in ideal pyrochlore structure, but is relatively much smaller than those in cotunnite-type $A_2B_2O_7$ structure, suggesting that the fluorite phase has more covalent character than the cotunnite-type structure.[37] In the cotunnite-type structure, coordination number of metal ions is generally 8- or 9-fold, whereas in the fluorite-type structures, metal ions coordinate with oxygen ion in 7- or 8-fold coordination. This suggests $La_2Hf_2O_7$ has the tendency to form ionic bonding with higher coordination number at high uranium doping concentration. Furthermore, based on Raman spectroscopy data, the increase of uranium doping level induces the gradual phase transformation from pyrochlore to fluorite and then cotunnite as observed by the appearance of broad peaks at 307 and 715 cm^{-1}. Zhang *et al.* have also observed such process in U doped $Gd_2Zr_2O_7$ but by applying pressure of 22 GPa, which finally transformed into a disordered fluorite structure on release of pressure.[28]

As a quantitative measure of the extent of anion disordering in the $La_2Hf_2O_7$:U NPs as a function of uranium doping concentration, the ratio of integrated Raman intensity between Raman active vibration mode of the distorted HfO_6 octahedra and the main F_{2g} Raman mode at $\omega_0 \approx 307\ cm^{-1}$ is plotted in **Figure 1b**.[38] Moreover, we annealed our samples at high temperature to enhance cation ordering and reduce strain, but there was little effect on the Raman spectra of our $La_2Hf_2O_7$:U NPs.[39] Thus, this ratio selectively indicates disorder on the anion sub-lattice.

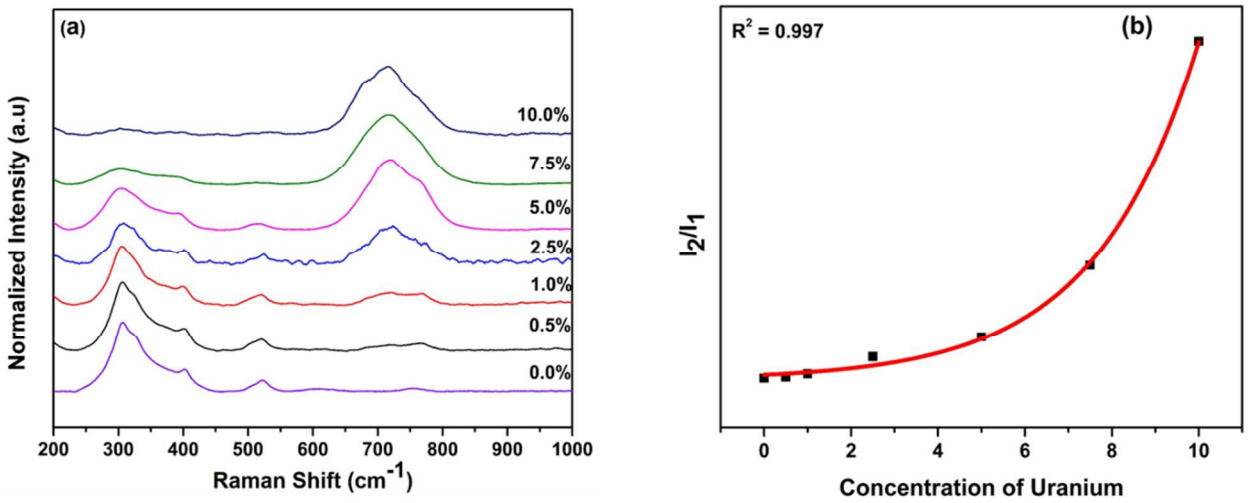

Figure 1. (a) Raman spectra of the $La_2Hf_2O_7$:x%U NPs (x = 0, 0.5, 1, 2.5, 5, 7.5, and 10) and (b) corresponding integrated Raman intensity ratio of the distorted HfO_6 octahedra (I_2) and the main F_{2g} Raman mode of the ordered pyrochlore (I_1). This Raman intensity ratio serves as a qualitative indicator of the progression of anion disorder as a function of uranium doping concentration in the $La_2Hf_2O_7$ host.

3.3 XPS Analysis

To confirm the oxidation state of uranium ion and other constituent elements in the $La_2Hf_2O_7$:U NPs, XPS was carried out for the lowest and highest composition. **Figure S8** depicts the XPS spectra of La 3d, Hf 4f and O 1s core level electron for the $La_2Hf_2O_7$:U NPs at various doping levels. **Figure S8a** shows the La 3d XPS spectra that indicated the binding energies (BE) values for La $3d_{5/2}$ and La $3d_{3/2}$ are approximately 839.7 and 852 eV in addition to satellite peaks at 865.6 and 877.4 eV at 0.5 % uranium doping. The La 3d X-ray photoelectron peak splits into $3d_{5/2}$ and $3d_{3/2}$ due to strong orbit coupling. There may be some additional contribution of ligand to metal charge transfer (oxygen to hafnium) which cause further splitting to these lines.[40] The BE difference in $3d_{3/2}$ and $3d_{5/2}$ states is around 16.5 eV, which indicates the stabilization of lanthanum ion in +3 oxidation state.[41] Most of the report on XPS spectra of HfO_2 [42-44] clearly shows spin-orbit coupling induced splitting in Hf 4f peak to $4f_{7/2}$ and $4f_{5/2}$ similar to what we have observed in our $La_2Hf_2O_7$:U NPs (**Figure S8b**). The BE values for these two peaks is approximately around BE = 18.9 eV and BE = 20.6 eV for 0.5 % uranium doped $La_2Hf_2O_7$ NPs with 4f spin-orbit splitting energy values around ~1.92 eV. All these data are in concordance with Hf in +4-oxidation state. Although it can be seen from **Figure S8b** that the Hf 4*f* peaks

become more pronounced for the higher doping concentrations of U, due to the overlap between the La 5*p* and Hf 4*f* spectra, the peak contributions are not clear. On increasing the concentration of uranium ion, there is slight variation in peak position for x-ray photoelectron of La-3d and Hf-4f due to slight doping inducing change in electronic localization as well as density. The Hf 4*p* and U 4*f* spectra have overlapping peaks. The O1s XPS spectra are shown in **Figure S3c**. As to-be-confirmed by PL data that there is uranium distribution (both U^{4+} and U^{6+}) at both La^{3+}/Hf^{4+} site, there are large density of charge compensating defect formation in our $La_2Hf_2O_7$:U NPs to take care of charge neutrality. One of predominant defects would be oxygen vacancy. The area under the surface hydroxyl/under-coordinated O 1s peak (O_v) is increasing with uranium doping concentration, suggesting the formation of oxygen vacancies due to charge neutrality.

Since XPS studies can distinguish different oxidation states of uranium according to the binding energy of 4f orbit, we have used XPS to confirm the oxidation state of uranium in our $La_2Hf_2O_7$ NPs (**Figure 2a**). From the XPS analysis, we confirmed the presence of both U^{4+} and U^{6+} in all samples with different concentrations. At higher concentrations the XPS spectra displayed two peaks at binding energies values of 382.5 and 393.3 corresponding to U $4f_{7/2}$ and U $4f_{5/2}$, respectively. This difference is because of spin orbit coupling. However, at lower doping concentrations (0.5%, and 1%) the U $4f_{5/2}$ peak is was absent. Because the U $4f_{5/2}$ peak was not observed at lower concentrations, we were unable to calculate the fractional ratio of U^{4+} and U^{6+} species in the 0.5% and 1% uranium doped $La_2Hf_2O_7$:U samples. The XPS parameters as calculated for the rest of the samples are shown in **Table S2**. From the ratio analysis, it is clearly evident that as the concentration of uranium dopant increases, there is an exponential decrease in the U^{4+}/U^{6+} ratio (**Figure 2b**), confirming that U^{4+} is dominating at lower concentrations, while at higher concentrations it is U^{6+}. This observation is consistent with our PL emission spectroscopy and lifetime studies as discussed in the next section.

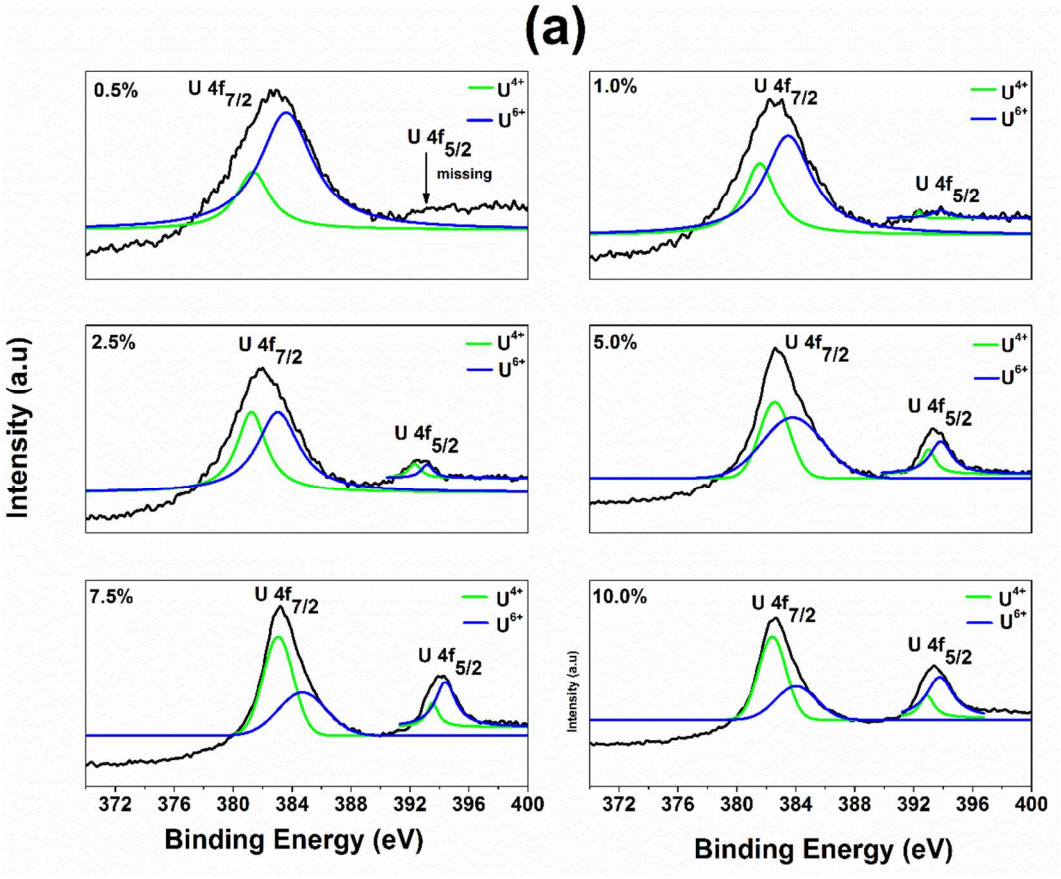
(a)
0.5%
1.0%
2.5%
5.0%
7.5%
10.0%
U 4f7/2
U 4f5/2
missing
U4+
U6+
Intensity (a.u)
372 376 380 384 388 392 396 400
Binding Energy (eV)

200

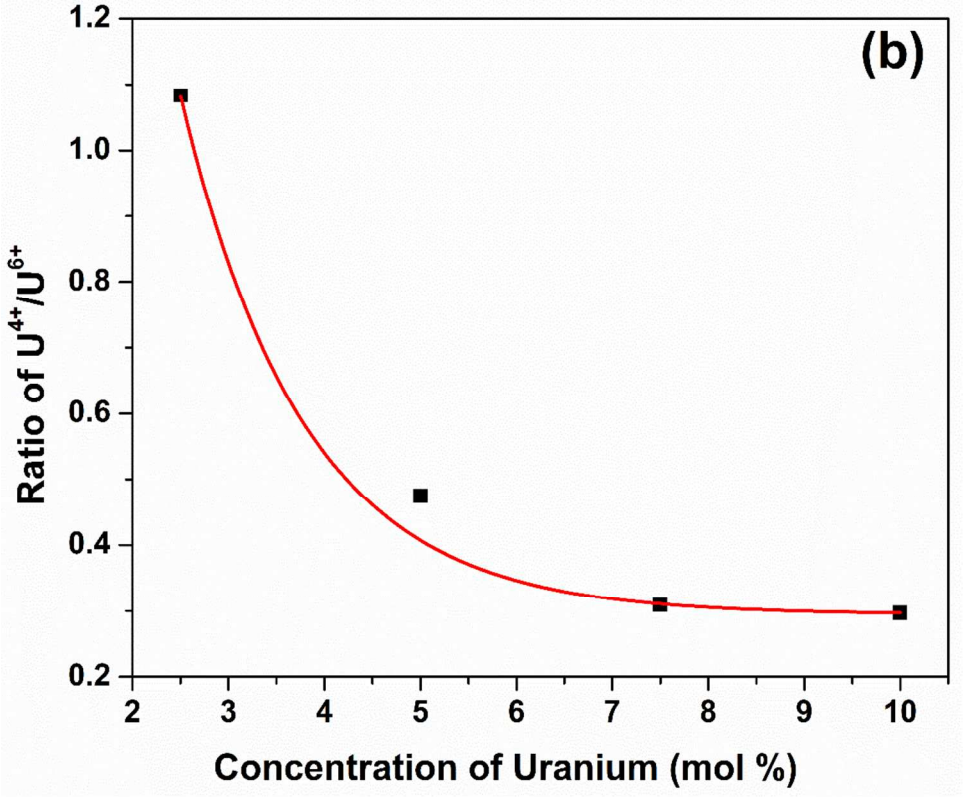
(b)
Ratio of U4+/U6+
1.2
1.0
0.8
0.6
0.4
0.2
2 3 4 5 6 7 8 9 10
Concentration of Uranium (mol %)

201

Figure 2. (a) Uranium $4f_{7/2}$ XPS spectra of the $La_2Hf_2O_7$:U NPs at different doping levels and (b) variation of the U^{4+}/U^{6+} ratio as a function of uranium doping levels (2.5-10 %).

3.4 Photoluminescence

3.4.1 Emission and excitation spectroscopy

PL emission spectra (Figure 3a) of the $La_2Hf_2O_7$:x%U (x = 0.5, 1.0, 2.5, 5.0, 7.5, and 10) NPs at λ_{ex} = 230 nm showed two different features in region a (Ra: 440 - 500 nm) and region b (Rb: 540 – 570 nm). In Ra, there is a cluster of four observable featureless bands centered at 451, 468, 482 and 493 nm in the blue region. In Rb, there is a single broadband at 550 nm in the green region.

The cluster of four bands in blue region is definitely not arising because of uranyl ions as they have unique signature of equally spaced vibronically coupled emission band whose value is close to symmetric stretching Raman mode of uranyl ion. Moreover, the position of the first band in the emission spectrum ($\upsilon_{0\text{-}0}$) is a unique signature for deciding the number of oxygen atom coordinated to uranium and its bond order, which is known as zero phonon line (ZPL). It corresponds to the electronic transition from triplet $^3\Pi_u$ state to singlet $^1\Sigma_g^+$ ($D_{\infty h}$) state from oxygen to the non-bonding orbital of uranium ($5f\delta_u$ and $5f\varphi_u$). In our spectrum, it is located at 451 nm, which is much lower than the normally observed in case of UO_2^{2+}.[45-47] This feature further supports the fact that the sharp features in Ra region corresponds to uranium in +4 oxidation state. It has been also reported previously that uranium has high tendency to be stabilized in both U^{+4} and U^{5+}/U^{+6} in $A_2B_2O_7$ type pyrochlore oxides.[48-49] Indeed, in our earlier work on U doped $Gd_2Zr_2O_7$, we could confirm that uranium has a tendency to stabilize in both U(4+) and U(6+) states.[24] In our case here, the emission peaks in region Ra are attributed to f→f transitions of the U^{4+} $5f^2$ ion.[24, 50-52] The spectral splitting of the U(IV) bands is the result of ligand field induced by hafnate ion. This particular emission is attributed to the relaxation of the highest energy $^3F_2$ charge-transfer excited-state manifold ($5f^16d^1$) to Russell-Saunders coupled $^3H_4(5f^2)$ ground state and higher lying energy states derived from the $5f^2$ electronic configuration.[24]

On the other hand, the broad peak in the green emission zone Rb at 550 nm is originated from uranium ion in +6 oxidation state, which allowed for oxygen to uranium charge transfer.[23-25, 45-47, 53-54] Therefore, it is due to ligand to metal charge transfer (LMCT) transition and is typical of uranium stabilizing in octahedral uranate ion UO_6^{6-}.[23, 53] Visible emission in the green region

emerges due to ligand to metal charge transfer (LMCT) involving bonding oxygen orbitals (Π_u, Π_g, Ω_g, and Ω_u) to nonbonding $5f_\delta$ and $5f_\Phi$ orbitals of uranium ion.

Apparently, uranyl ion (UO_2^{2+}) vibronic features are very distinct from those that arises due to LMCT transitions. Normally LMCT induced vibronic transitions are very broad and often structureless. It is very difficult to identify the zero-phonon lines (ZPLs) and vibration modes from there. This is because of the fact that broadening due to LMCT induces lattice displacements and charge-hole relaxation in the valence band.[55] Previously published work has shown that uranyl ion has a unique emission peak with constant spacing.[23-25, 45-47, 53-54] The origin of such vibronic coupling is the strong interaction of the ground state Raman active O=U=O symmetric stretching mode with the $^3\Pi_u$ electronic triplet excited state (generally observed between 780 and 900 cm^{-1}). Isolated uranyl ion has three Raman active modes at ground state vibrational frequencies of 830 (ω_2), 920 (ω_2) and 250 (ω_3) cm^{-1} due to symmetric stretching, asymmetric stretching and bending, respectively. However, based on Franck Condon principle only symmetric stretching modes are allowed to couple with the electric dipole transition of uranyl ion.[56] Therefore, as a unique signature of the uranyl ion, vibronic band progresses harmonically in the frequency of the O=U=O symmetric stretching. These are known as false origins:[57] ω_2 and ω_2 are coupled to the vibronic transitions of the symmetric stretching mode that progress in the frequency of ω_1. No harmonics of asymmetric stretching ω_2 and bending mode ω_3 appear in the uranyl vibronic spectra because they are non Franck-Condon mode. Absence of such signature clearly rules out the stabilization of uranium ion as UO_2^{2+} in $La_2Hf_2O_7$.

Among various stable forms, hexavalent uranium ions depending on the conditions of concentration, annealing temperature, and structure of host can have different molecular structures leading to tetrahedral uranate UO_4^{2-}, octahedral uranate UO_6^{6-} or uranyl UO_2^{2+} species. Of these uranyl ions, UO_2^{2+} ions have been studied most extensively, because it is the most prevalent form of natural uranium in the ecological system. Uranyl ions are characterized by uranium-oxygen partial triple bond character, whereas octahedral and tetrahedral uranate ions are characterized by uranium-oxygen single bond. Crystal lattice hosts that favor the formation of U-O bond (singly bonded) will stabilize uranium ion in the form of uranate ions while those that offer close packed environments favor shorter triply bonded uranium-oxygen bonds to stabilize uranium in the form of UO_2^{2+} ions.[58] From our earlier work on magnesium aluminate spinel and strontium silicate,[45-46] uranium stabilizes as UO_2^{2+} in $MgAl_2O_4$ whereas as both U (+4) and

UO_6^{6-} in $Gd_2Zr_2O_7$.[24] On the other hand, it tends to stabilize as UO_6^{6-} in $SrZrO_3$, $Nd_2Zr_2O_7$, and Sr_2CeO_4.[23, 53-54] In this case here, uranium stabilizes as both +4 and + 6 oxidation state in the form of U^{4+} ion as well as UO_6^{6-} ion at 1.0 % uranium doped $La_2Hf_2O_7$.

The representative excitation bands corresponding to U^{4+} and UO_6^{6-} emissions were taken from the $La_2Hf_2O_7$:1.0mol%U NPs (**Figure 3b**). The distinct features in the two cases are another indication of the fact that the emission features in blue and green region has different origin altogether. The shoulder around 200-250 nm is attributed to oxygen to uranium charge transfer transition whereas the fine structure from 300-400 nm is the intra f-f band of uranium ion.

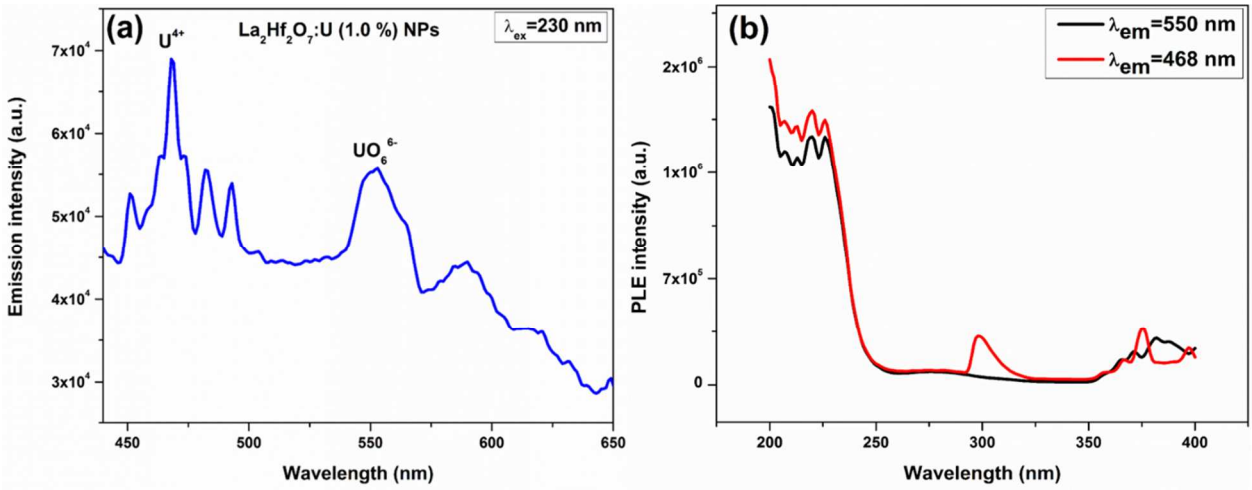

Figure 3. (a) Emission spectrum and (b) excitation spectrum of the $La_2Hf_2O_7$:1.0mol%U NPs.

Figure 4a depicts the emission spectra of the $La_2Hf_2O_7$:U NPs for various uranium concentrations and **Figure 4b** displayed the effect of uranium ion concentration on emission intensity for both U^{4+} emission at 458 nm and UO_6^{6-} emission at 550 nm. The emission intensity increases up to 1.0 % uranium doping, and after that, there is an emission intensity reduction. Such phenomenon is attributed to concentration quenching. At higher doping concentration, the distance between two-activator ions decreased to an extent where non-radiative energy transfer between them is facilitated. That distance in photophysical parlance is called critical distance. To confirm the non-radiative energy transfer mechanism, which leads to concentration quenching, critical distance (R_c) needs to be determined using the following equation:

$$R_c = 2\left(\frac{3V}{4\pi X_c N}\right)^{\frac{1}{3}}$$

where R_c is called critical distance and is defined as the minimum possible distance between the dopant ions at which non-radiative energy transfer takes place, V is the volume of the unit cell,

286 X_c is the critical concentration of dopant ion, and N is the number of cations present in one
287 formula unit of host. The values of V and N for $La_2Hf_2O_7$ are 1250.32 $Å^3$ and 16, respectively.
288 Considering X_C = 1.0% (0.01), critical energy transfer distance R_c in the $La_2Hf_2O_7$:1.0%U NPs
289 was estimated to be 24.62 Å. In this case, non-radiative energy transfer takes place at the U-U
290 distance greater than 10 Å via electric multipolar interaction.
291 In addition, uranium was stabilized as both U^{4+} and UO_6^{6-} ions in all doping concentrations in the
292 $La_2Hf_2O_7$ host, but their relative intensity changes (**Figure 4a**). At low concentrations, the
293 fraction of U^{4+} is more than that of UO_6^{6-} whereas the trends reverses at high doping
294 concentrations as plotted in **Figure 4c**. This in an interesting observation consistent with XPS
295 data, which can be correlated to some kind of structural changes. At low uranium doping,
296 $A_2B_2O_7$ structure favors the stabilization of U^{4+} over that of UO_6^{6-}. At high doping level, $A_2B_2O_7$
297 structure favors UO_6^{6-} over U^{4+}. It has been reported that the structure of host materials plays
298 huge roles in stabilizing different oxidation states and coordinations of doping ions. Perovskite
299 structure tends to stabilize the U(VI) oxidation state in UO_6^{6-} coordination[53] whereas spinel
300 structure tends to favor the same oxidation state but in a different geometry as UO_2^{2+} ion.[45] On
301 the other hand, fluorite type $A_2B_2O_7$ composition favors the stabilization of both U^{4+} and U^{6+}.[24]
302 In this case, our Raman spectroscopy results are assimilate our PL observations, supporting the
303 fact that oxidation stabilization of uranium is dependent on the structural and phase evolution of
304 the NPs.

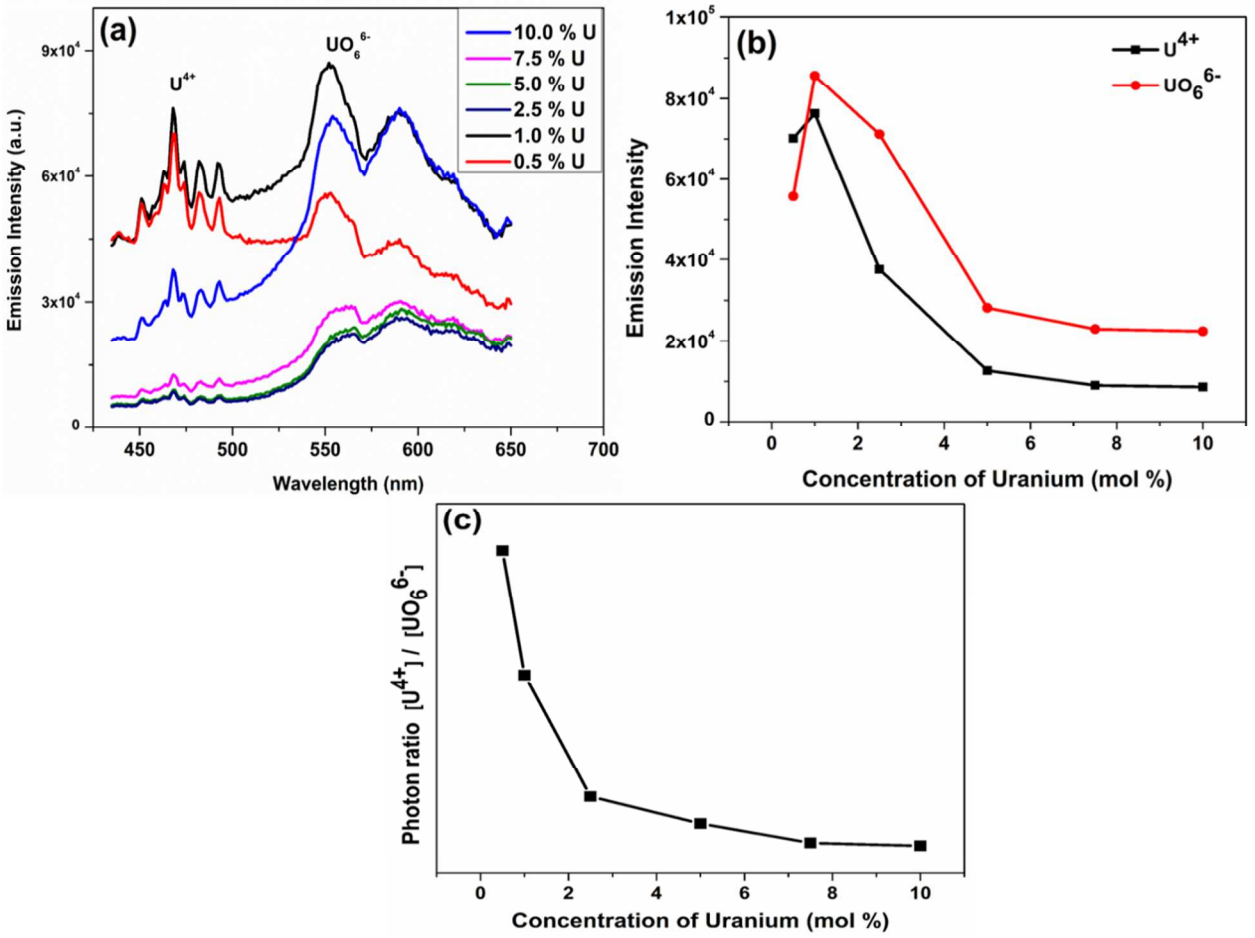

Figure 4. (a) Emission spectra of the $La_2Hf_2O_7$:U NPs with various uranium doping concentrations with λ_{ex} = 230 nm, and (b) corresponding plot of emission intensity and (c) ratio of emission intensity from the U^{4+} and UO_6^{6-} ions as a function of the uranium doping concentration.

3.4.2 Lifetime spectroscopy

Investigating the local site occupied by U ions in the $A_2B_2O_7$ type pyrochlore structure is very important from the point of view of nuclear waste immobilization. In ideal pyrochlore lattice, there are two cationic sites having 16*c* and 16*d* Wyckoff positions with different coordination numbers (CNs). In addition, there are two anionic sites at 8*a* and 48*f* Wyckoff positions. Dopant ion occupancy on these sites depends on their ionic radii. The 16*c* cation site having CN of six anions on the 48*f* sites and two on the 8*a* sites is usually occupied by large size dopant ions, whereas the 16*d* cationic site having CN of six anions on the 48*f* sites is usually occupied by small sized ions[28].

As far as ionic radius is concerned, uranium in 8-coordination (100 pm) is shorter than 8-coordinated La^{3+} ion (116 pm), so it can easily reside on the lanthanum site. On the other hand, 6-coordinated Hf^{4+} ion (71 pm) is smaller, and its site is difficult to accommodate large sized uranium ion (89 pm). On the other hand, for U^{4+} ion substitution, Hf^{4+} site favors charge matching whereas there is a need for charge compensation at La^{3+} site. Charge matching is energetically more favorable situation than size matching. Therefore, U^{4+} ion feels less distortion at Hf^{4+} site relative to at La^{3+} site due to its same ionic charge with Hf^{4+} ion. Therefore, room temperature luminescence decay profiles of the $La_2Hf_2O_7$:1.0%U NPs were measured with emission wavelengths of 468 nm and 552 nm after excited at 230 nm (**Figure 5a and b**). The luminescence decay profile corresponding to U^{4+} ion (468 nm) displayed a biexponential behavior with two lifetime values (ESI). It indicates that U^{4+} ion is not homogeneously distributed in the $La_2Hf_2O_7$ matrix.

Based on the fitting data, the decay curve shows two different lifetime values of 1.01 and 9.68 µs with magnitudes 60% and 40%, respectively. The long lifetime measured from the $La_2Hf_2O_7$:1.0%U NPs (9.68 µs) is ascribed to uranate ion localized at the La^{3+} site whereas the fast decaying uranyl ion (1.01 µs) is attributed to U^{4+} ion localized at Hf^{4+} site. The PL decay profile corresponding to UO_6^{6-} ion (550 nm) also displayed a biexponential behavior with lifetime values of 1.01 µs (39%) and 9.09 µs (61%). Here the fast decaying uranium is attributed to U(IV) ion localized at the Hf^{4+} site whereas the slow decaying uranium ion is attributed to UO_6^{6-} ion at La^{3+} site. In this case, one U^{6+} ion replaces two La^{3+} sites and charge-compensating defects are cation vacancies.

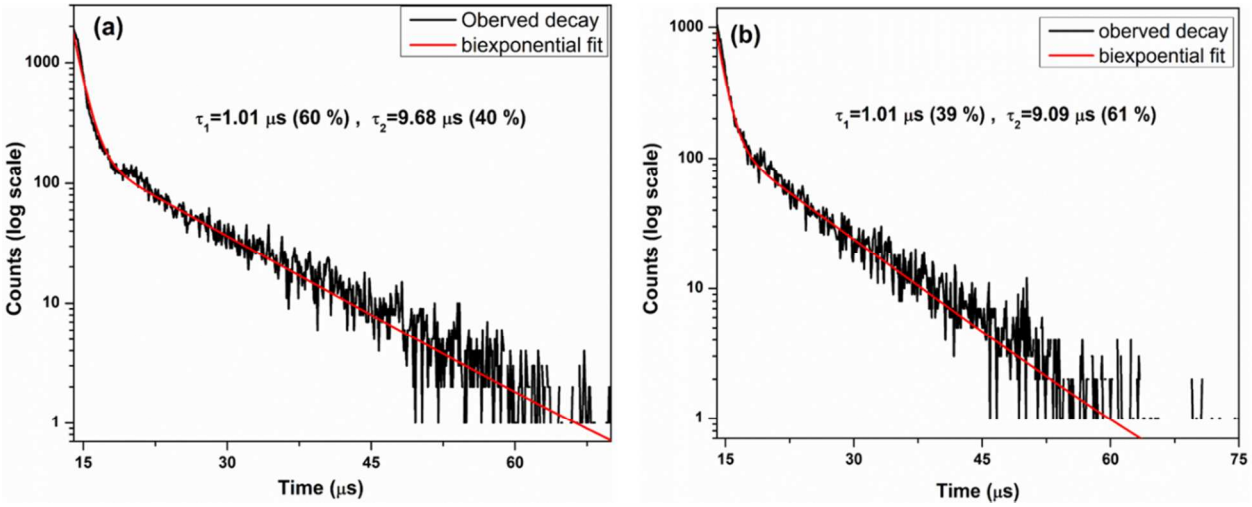

Figure 5. Luminescence decay profiles of the $La_2Hf_2O_7$:1.0%U NPs with emission wavelengths of (a) 468 nm and (b) 552 nm after excited at 230 nm.

3.5 Structural evolution of the $La_2Hf_2O_7$:10%U NPs by In-situ Raman spectroscopy

To further investigate the structural evolution of our $La_2Hf_2O_7$:x%U NPs, we took in-situ Raman spectra of $La_2Hf_2O_7$:10%U NPs as an example with our initial effort. From the discussion above, the $La_2Hf_2O_7$:10%U NPs exists in complete cotunnite structure. The average metal-oxygen bond length in the fluorite-phase is much closer to those existing in ideal pyrochlore structures, but is relatively much smaller than that in cotunnite-type $A_2B_2O_7$ structures, suggesting that the fluorite phases have more covalent character than the cotunnite-type[37]. In the cotunnite-type structure though, coordination number of metal ion is generally 8 or 9-fold whereas in the fluorite-type structures metal ion coordinates with oxygen ion in 7 or 8 fold coordination. This suggest that at high uranium concentration hafnate pyrochlore has tendency to form ionic bonding with higher coordination number.

With increasing temperature from 25°C to 950°C (**Figure 6a**), this particular the $La_2Hf_2O_7$:10%U sample underwent phase transformation from cotunnite phase to ordered pyrochlore phase. At the highest reached measurement temperature, i.e. 950°C, all the Raman modes expected for ordered pyrochlore phase were found from the heated sample with the almost complete disappearance of the 715 cm^{-1} peak originated from the structurally disorder cotunnite phase (top panel of **Figure 6a**) while the disordered fluorite phase was probably unseen. The complete phase transformation took place around 900^{o}C. Even more interestingly and for the first time, we found that the phase change is reversible, i.e., the Raman band corresponding to cotunnite phase reappear after the sample was cooled down back to room temperature (**Figure 6b**). With the initial exciting Raman results collected so far, further investigations are undergoing, including in-situ Raman studies of other composition along with in-situ PL, X-ray absorption spectroscopy and neutron diffraction measurements, and will be reported separately in the near future.

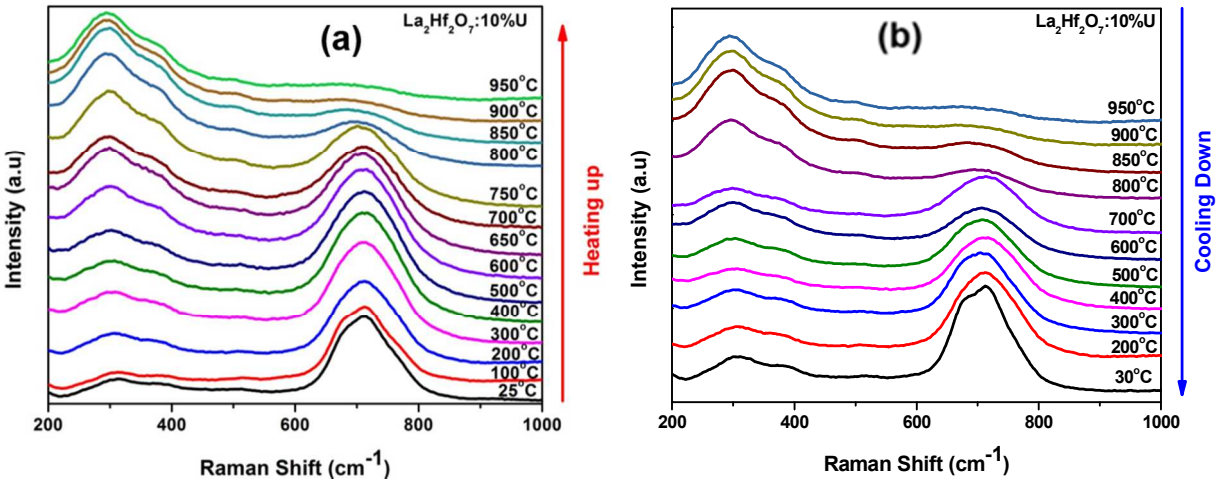

Figure 6. In-situ Raman spectra of the $La_2Hf_2O_7$:10%U NPs in consecutive heating and cooling cycle.

4. Conclusion

In this work, uranium doped $La_2Hf_2O_7$ nanoparticles were successfully synthesized using a combined co-precipitation and molten salt synthesis method. XRD and FTIR demonstrated the formation of pure $La_2Hf_2O_7$ phase with particle size in the nanodomain as confirmed using electron microscopy. Emission and lifetime spectroscopy further suggested the existence of U^{4+} ions along with U^{6+} ions as UO_6^{6-} species. The same has been further corroborated by more oxidation state sensitive XPS. Luminescence lifetime measurement confirmed the stabilization of fast decaying U^{4+} at Hf^{4+} site whereas slowly decaying U^{6+} tends to stabilize at La^{3+} site. Further concentration dependence studies showed maximum emission output for 1.0 % uranium doped samples and the concentration quenching in these NPs was attributed to non-radiative energy transfer via multipolar interaction. Another interesting phenomenon was observed from the emission spectra as well as XPS: at low uranium doping concentration, the proportion of U^{4+} ion was more than that of U^{6+}, whereas at high uranium doping concentration, the opposite happened. We successfully explained this phenomenon using Raman spectroscopy, which demonstrated a structural phase transition from order pyrochlore to cotunnite with increasing uranium doping concentration. It was concluded that ordered pyrochlore phase favors uranium stabilization in +4-valence state whereas disordered cotunnite phase energetically favors octahedral uranate ions UO_6^{6-}. To further understand the structural evolution, in-situ Raman measurements were carried out on the $La_2Hf_2O_7$:10%U NPs between room temperature and

950°C. A reversible structural transition was found at 900°C between ordered pyrochlore phase and disorder cotunnite phase. Therefore, it is expected that this work open new research areas of fundamental solid-state spectroscopy of uranium, doping induced pyrochlore to fluorite phase transition, and structure-optical property correlation in doped $A_2B_2O_7$ with urgent importance to nuclear power industry and sustainable environment.

Acknowledgement

The authors thank the financial support by the National Science Foundation under CHE (award #1710160) and DMR (grant #1523577) and the USDA National Institute of Food and Agriculture (award #2015-38422-24059, for the Integrating Food Science/Engineering and Education Network (IFSEEN) program). The Department of Chemistry at the University of Texas Rio Grande Valley is grateful for the generous support provided by a Departmental Grant from the Robert A. Welch Foundation (Grant No. BX-0048). SKG would like to thanks United States-India Education Foundation (USIEF) and Institute of International Education (IIE) for his Fulbright Nehru Postdoctoral Fellowship (Award# 2268/FNPDR/2017). The in-situ Raman measurements were conducted at the Center for Nanophase Materials Science, which is a DOE Office of Science User Facility, and the authors thank Dr. A. Puretzky for technical assistance. Authors would also like to thank Ms. Melonie Thomas for HRTEM and Pragathi Darapaneni, Louisiana State University for XPS measurements.

References

1. Zhang, S.; Zhang, H.; Zhao, F.; Jiang, M.; Xiao, H.; Liu, Z.; Zu, X., Impact of isovalent and aliovalent substitution on the mechanical and thermal properties of $Gd_2Zr_2O_7$. *Scientific reports* **2017,** *7*, 6399.
2. Feng, Y.; Zhu, S.; Bian, J.; Chen, F.; Chen, S.; Ma, C.; Liu, H.; Fang, B., Magnetic and electrical transport properties of the pyrochlore iridate $Bi_{2-x}Co_xIr_2O_7$. *Journal of Magnetism and Magnetic Materials* **2018,** *451*, 283-287.
3. Radha, R.; Kumar, R.; Sakar, M.; Balakumar, S., Understanding the lattice composition directed in situ structural disorder for enhanced visible light photocatalytic activity in Bismuth iron niobate pyrochlore. *Applied Catalysis B: Environmental* **2018,** *225*, 386-396.
4. Pokhrel, M.; Wahid, K.; Mao, Y., Systematic studies on $RE_2Hf_2O_7$:5% Eu^{3+}(RE=Y, La, Pr, Gd, Er, and Lu) nanoparticles: effects of the A-site RE^{3+} cation and calcination on structure and photoluminescence. *The Journal of Physical Chemistry C* **2016,** *120*, 14828-14839.
5. Mustafa, G. M.; Atiq, S.; Abbas, S. K.; Riaz, S.; Naseem, S., Tunable structural and electrical impedance properties of pyrochlores based Nd doped lanthanum zirconate nanoparticles for capacitive applications. *Ceramics International* **2018,** *44*, 2170-2177.

6. Zhang, K.; He, Z.; Peng, L.; Zhang, H.; Lu, X., Self-propagating synthesis of $Y_{2-x}Nd_xTi_2O_7$ pyrochlore and its aqueous durability as nuclear waste form. *Scripta Materialia* **2018,** *146*, 300-303.
7. Vorozhtcov, V. A.; Stolyarova, V. L.; Lopatin, S. I.; Simonenko, E. P.; Simonenko, N. P.; Sakharov, K. A.; Sevastyanov, V. G.; Kuznetsov, N. T., Vaporization and thermodynamic properties of lanthanum hafnate. *Journal of Alloys and Compounds* **2018,** *735*, 2348-2355.
8. Zhou, G.; Wang, Z.; Zhou, B.; Zhao, Y.; Zhang, G.; Wang, S., Fabrication of transparent $Y_2Hf_2O_7$ ceramics via vacuum sintering. *Optical Materials* **2013,** *35*, 774-777.
9. Wahid, K.; Pokhrel, M.; Mao, Y., Structural, photoluminescence and radioluminescence properties of Eu^{3+} doped $La_2Hf_2O_7$ nanoparticles. *Journal of Solid State Chemistry* **2017,** *245*, 89-97.
10. An, L.; Ito, A.; Goto, T., Fabrication of transparent $Lu_2Hf_2O_7$ by reactive spark plasma sintering. *Optical Materials* **2013,** *35*, 817-819.
11. Alice, M. D.; Peter, K.; Corruccini, L. R., Heat capacity of the frustrated magnetic pyrochlores $Gd_2Zr_2O_7$ and $Gd_2Hf_2O_7$. *Journal of Physics: Condensed Matter* **2008,** *20*, 235208.
12. Gu, S.; Zhang, S.; Xu, D.; Li, W.; Yan, J., Evolution of microstructure and hot corrosion performance of $La_2Hf_2O_7$ ceramic in contact with molten sulfate-vanadate salt. *Ceramics International* **2018,** *44*, 2048-2057.
13. Ji, Y.; Jiang, D.; Shi, J., $La_2Hf_2O_7$:Ti^{4+} ceramic scintillator for x-ray imaging. *Journal of materials research* **2005,** *20*, 567-570.
14. Hansel, R. A.; Desai, S.; Allison, S. W.; Heyes, A.; Walker, D. G., Emission lifetimes of europium-doped pyrochlores for phosphor thermometry. AIP: 2010; Vol. 107, p 016101.
15. Lumpkin, G. R.; Whittle, K. R.; Rios, S.; Smith, K. L.; Zaluzec, N. J., Temperature dependence of ion irradiation damage in the pyrochlores $La_2Zr_2O_7$ and $La_2Hf_2O_7$. *Journal of Physics: Condensed Matter* **2004,** *16*, 8557.
16. Hashem, E.; Platts, J. A.; Hartl, F. e.; Lorusso, G.; Evangelisti, M.; Schulzke, C.; Baker, R. J., Thiocyanate complexes of uranium in multiple oxidation states: A combined structural, magnetic, spectroscopic, spectroelectrochemical, and theoretical study. *Inorganic chemistry* **2014,** *53*, 8624-8637.
17. Natrajan, L. S., Developments in the photophysics and photochemistry of actinide ions and their coordination compounds. *Coordination Chemistry Reviews* **2012,** *256*, 1583-1603.
18. Sobczyk, M.; Drożdżyński, J.; Lisiecki, R.; Ryba-Romanowski, W., Near infrared and visible luminescence of U^{3+}-doped $PbCl_2$ single crystals. *Journal of Luminescence* **2008,** *128*, 185-189.
19. Steudtner, R.; Arnold, T.; Großmann, K.; Geipel, G.; Brendler, V., Luminescence spectrum of uranyl (V) in 2-propanol perchlorate solution. *Inorganic Chemistry Communications* **2006,** *9*, 939-941.
20. Zhang, Y.; Kong, L.; Aughterson, R. D.; Karatchevtseva, I.; Zheng, R., Phase evolution from $Ln_2Ti_2O_7$ (Ln= Y and Gd) pyrochlores to brannerites in glass with uranium incorporation. *Journal of the American Ceramic Society* **2017,** *100*, 5335-5346.
21. Shu, X.; Fan, L.; Xie, Y.; Zhu, W.; Pan, S.; Ding, Y.; Chi, F.; Wu, Y.; Lu, X., Alpha-particle irradiation effects on uranium-bearing $Gd_2Zr_2O_7$ ceramics for nuclear waste forms. *Journal of the European Ceramic Society* **2017,** *37*, 779-785.
22. Lu, X.; Hou, C.; Xie, Y.; Shu, X.; Ding, Y.; Ma, D.; Ren, W.; Bian, L., High capacity immobilization of U_3O_8 in $Gd_2Zr_2O_7$ ceramics via appropriate occupation designs. *Ceramics International* **2017,** *43*, 3015-3024.
23. Gupta, S. K.; Reghukumar, C.; Keskar, M.; Kadam, R., Revealing the oxidation number and local coordination of uranium in $Nd_2Zr_2O_7$ pyrochlore: A photoluminescence study. *Journal of Luminescence* **2016,** *177*, 166-171.
24. Gupta, S. K.; Reghukumar, C.; Pathak, N.; Sudarshan, K.; Tyagi, D.; Mohapatra, M.; Pujari, P.; Kadam, R., Speciation of uranium and doping induced defects in $Gd_{1.98}U_{0.02}Zr_2O_7$: Photoluminescence, X-ray photoelectron and positron annihilation lifetime spectroscopy. *Chemical Physics Letters* **2017,** *669*, 245-250.

25. Mohapatra, M.; Rajeswari, B.; Hon, N.; Kadam, R., Uranium luminescence in $La_2Zr_2O_7$: effect of concentration and annealing temperature. *Luminescence* **2016,** *31*, 1519-1523.
26. Kutty, K. G.; Asuvathraman, R.; Madhavan, R. R.; Jena, H., Actinide immobilization in crystalline matrix: a study of uranium incorporation in gadolinium zirconate. *Journal of Physics and Chemistry of Solids* **2005,** *66*, 596-601.
27. Shu, X.; Lu, X.; Fan, L.; Yang, R.; Ding, Y.; Pan, S.; Zhou, P.; Wu, Y., Design and fabrication of $Gd_2Zr_2O_7$-based waste forms for U_3O_8 immobilization in high capacity. *Journal of materials science* **2016,** *51*, 5281-5289.
28. Zhang, F.; Lang, M.; Tracy, C.; Ewing, R. C.; Gregg, D. J.; Lumpkin, G., Incorporation of uranium in pyrochlore oxides and pressure-induced phase transitions. *Journal of Solid State Chemistry* **2014,** *219*, 49-54.
29. Phillips, M. C.; Brumfield, B. E.; LaHaye, N.; Harilal, S. S.; Hartig, K. C.; Jovanovic, I., Two-dimensional fluorescence spectroscopy of uranium isotopes in femtosecond laser ablation plumes. *Scientific reports* **2017,** *7*, 3784.
30. Mao, Y.; Guo, X.; Huang, J. Y.; Wang, K. L.; Chang, J. P., Luminescent nanocrystals with $A_2B_2O_7$ composition synthesized by a kinetically modified molten salt method. *The Journal of Physical Chemistry C* **2009,** *113*, 1204-1208.
31. Mao, Y.; Park, T. J.; Zhang, F.; Zhou, H.; Wong, S. S., Environmentally friendly methodologies of nanostructure synthesis. *Small* **2007,** *3*, 1122-1139.
32. Turner, K. M.; Rittman, D. R.; Heymach, R. A.; Tracy, C. L.; Turner, M. L.; Fuentes, A. F.; Mao, W. L.; Ewing, R. C., Pressure-induced structural modifications of rare-earth hafnate pyrochlore. *Journal of Physics: Condensed Matter* **2017,** *29*, 255401.
33. Subramanian, M.; Aravamudan, G.; Rao, G. S., Oxide pyrochlores—a review. *Progress in Solid State Chemistry* **1983,** *15*, 55-143.
34. Stanek, C.; Jiang, C.; Uberuaga, B.; Sickafus, K.; Cleave, A.; Grimes, R., Predicted structure and stability of $A_4B_3O_{12}\delta$-phase compositions. *Physical Review B* **2009,** *80*, 174101.
35. Garg, N.; Pandey, K.; Murli, C.; Shanavas, K.; Mandal, B. P.; Tyagi, A.; Sharma, S. M., Decomposition of lanthanum hafnate at high pressures. *Physical Review B* **2008,** *77*, 214105.
36. De los Reyes, M.; Whittle, K. R.; Zhang, Z.; Ashbrook, S. E.; Mitchell, M. R.; Jang, L.-Y.; Lumpkin, G. R., The pyrochlore to defect fluorite phase transition in $Y_2Sn_{2-x}Zr_xO_7$. *RSC Advances* **2013,** *3*, 5090-5099.
37. Xiao, H. Y.; Zhang, F.; Gao, F.; Lang, M.; Ewing, R. C.; Weber, W. J., Zirconate pyrochlores under high pressure. *Physical Chemistry Chemical Physics* **2010,** *12*, 12472-12477.
38. Rittman, D. R.; Turner, K. M.; Park, S.; Fuentes, A. F.; Park, C.; Ewing, R. C.; Mao, W. L., Strain engineered pyrochlore at high pressure. *Scientific reports* **2017,** *7*, 2236.
39. Fuentes, A. F.; Boulahya, K.; Maczka, M.; Hanuza, J.; Amador, U., Synthesis of disordered pyrochlores, $A_2Ti_2O_7$ (A= Y, Gd and Dy), by mechanical milling of constituent oxides. *Solid state sciences* **2005,** *7*, 343-353.
40. Pawlak, D. A.; Ito, M.; Oku, M.; Shimamura, K.; Fukuda, T., Interpretation of XPS O (1s) in mixed oxides proved on mixed perovskite crystals. *The Journal of Physical Chemistry B* **2002,** *106*, 504-507.
41. Zuniga, J. P.; Gupta, S. K.; Pokhrel, M.; Mao, Y., Exploring the optical properties of La2Hf2O7: Pr^{3+} nanoparticles under UV and X-ray excitation for potential lighting and scintillating applications. *New Journal of Chemistry* **2018**.
42. Pan, T.-M.; Chen, F.-H.; Shao, Y.-H., High-performance InGaZnO thin-film transistor incorporating a $HfO_2/Er_2O_3/HfO_2$ stacked gate dielectric. *RSC Advances* **2015,** *5*, 51286-51289.
43. Rudenja, S.; Minko, A.; Buchanan, D., Low-temperature deposition of stoichiometric HfO_2 on silicon: Analysis and quantification of the HfO_2/Si interface from electrical and XPS measurements. *Applied Surface Science* **2010,** *257*, 17-21.

44. Xie, H.; Liu, Q.; Li, Y.; Lv, H.; Wang, M.; Liu, X.; Sun, H.; Yang, X.; Long, S.; Liu, S., Nitrogen-induced improvement of resistive switching uniformity in a HfO_2-based RRAM device. *Semiconductor Science and Technology* **2012,** *27*, 125008.

45. Gupta, S. K.; Pathak, N.; Ghosh, P.; Kadam, R., On the photophysics and speciation of actinide ion in $MgAl_2O_4$ spinel using photoluminescence spectroscopy and first principle calculation: A case study with uranium. *Journal of Alloys and Compounds* **2017,** *695*, 337-343.

46. Gupta, S. K.; Yadav, A.; Nigam, S.; Jha, S.; Mazumder, C.; Bhattacharya, D.; Thulasidas, S., Speciation and site occupancy of uranium in strontium orthosilicate by photoluminescence and X-ray absorption spectroscopy: A combined experimental and theoretical approach. *Spectrochimica Acta Part A: Molecular and Biomolecular Spectroscopy* **2015,** *151*, 453-458.

47. Rout, A.; Panigrahi, B. S.; Nayak, C.; Bhattacharyya, D.; Jha, S. N., Uranium speciation and its site occupancy in alkaline-earth borophosphates. *Journal of the American Ceramic Society* **2017,** *100*, 2921-2931.

48. Gregg, D. J.; Zhang, Y.; Zhang, Z.; Karatchevtseva, I.; Blackford, M. G.; Triani, G.; Lumpkin, G. R.; Vance, E. R., Crystal chemistry and structures of uranium-doped gadolinium zirconates. *Journal of Nuclear Materials* **2013,** *438*, 144-153.

49. James, M.; Carter, M. L.; Zhang, Z.; Zhang, Y.; Wallwork, K. S.; Avdeev, M.; Vance, E. R., Crystal chemistry and structures of (Ca, U) titanate pyrochlores. *Journal of the American Ceramic Society* **2010,** *93*, 3464-3473.

50. Hashem, E.; Lorusso, G.; Evangelisti, M.; McCabe, T.; Schulzke, C.; Platts, J. A.; Baker, R. J., Fingerprinting the oxidation state of U (IV) by emission spectroscopy. *Dalton Transactions* **2013,** *42*, 14677-14680.

51. Hashem, E.; Swinburne, A. N.; Schulzke, C.; Evans, R. C.; Platts, J. A.; Kerridge, A.; Natrajan, L. S.; Baker, R. J., Emission spectroscopy of uranium (IV) compounds: a combined synthetic, spectroscopic and computational study. *RSC Advances* **2013,** *3*, 4350-4361.

52. Natrajan, L. S., The first structural and spectroscopic study of a paramagnetic 5f DO3A complex. *Dalton Transactions* **2012,** *41*, 13167-13172.

53. Gupta, S. K.; Pathak, N.; Gupta, R.; Thulasidas, S.; Natarajan, V., Probing the oxidation state and coordination geometry of uranium ion in $SrZrO_3$ perovskite. *Journal of Molecular Structure* **2014,** *1068*, 204-209.

54. Sahu, M.; Gupta, S. K.; Jain, D.; Saxena, M.; Kadam, R., Solid state speciation of uranium and its local structure in Sr_2CeO_4 using photoluminescence spectroscopy. *Spectrochimica Acta Part A: Molecular and Biomolecular Spectroscopy* **2018,** *195*, 113-119.

55. Liu, G.; Deifel, N. P.; Cahill, C. L.; Zhurov, V. V.; Pinkerton, A. A., Charge transfer vibronic transitions in uranyl tetrachloride compounds. *The Journal of Physical Chemistry A* **2012,** *116*, 855-864.

56. Liu, G.; Jensen, M., Theoretical analysis of optical spectra of uranyl in complexes. *Chemical Physics Letters* **2010,** *499*, 178-181.

57. Metcalf, D. H.; Dai, S.; Del Cul, G.; Toth, L., Luminescence spectra of single crystals of Cs_2ZrCl_6:$UO_2Cl_4^{2-}$ at low temperatures. vibronic structure of UO_2^{2+} doped in a cubic host. *Inorganic Chemistry* **1995,** *34*, 5573-5577.

58. Gupta, S. K.; Pathak, N.; Mohapatra, M.; Kadam, R. In *Role of lattice indeed plays a major role in uranium electronic structure: a case study with pyrochlore, spinel and perovskite*, Proceedings of the thirteenth DAE-BRNS nuclear and radiochemistry symposium, India, INIS: India, 2017.